

Is Sr_2RuO_4 a triplet superconductor?

K. Machida and M. Ichioka

Department of Physics, Okayama University, Okayama 700-8530, Japan

(Dated: February 1, 2008)

The field dependence of the specific heat $\gamma(H)$ at lower temperatures in Sr_2RuO_4 is analyzed by solving microscopic Eilenberger equation numerically. We find that systematic $\gamma(H)$ behaviors from a concave \sqrt{H} to a convex H^α ($\alpha > 1$) under H orientation change are understood by taking account of the Pauli paramagnetic effect. The magnetizations are shown to be consistent with it. This implies either a singlet pairing or a triplet one with d -vector locked in the basal plane, which allows us to explain other mysteries of this compound in a consistent way.

PACS numbers: 74.20.Rp, 74.70.Pq, 74.25.Op, 74.25.Bt

Superconductors are classified into two distinctive groups, either spin-singlet or spin-triple pairings. While almost all superconductors, including high T_c cuprates belong to the former, the later is extremely rare and difficult to find. Only a few examples of superconductors are discussed for its possibility; In a heavy Fermion material UPt_3 the identification of a triplet pairing has been firmly established [1, 2]. The observed multiple phase diagram in field (H) versus temperature (T) plane, consisting of three phases A, B and C, is reasonably explained only in terms of triplet pairing. This situation is similar to superfluid ^3He where two subphases ABM and BW are identified in pressure vs. T plane [3]. Knight shift (KS) experiment by NMR has played a fundamental role to confirm the theoretical predictions in UPt_3 . It was particularly crucial that both field directions where KS is changed and unchanged below T_c are found experimentally [4] as predicted [2], identifying the d -vector direction.

Sr_2RuO_4 is second prime candidate for a triplet pairing superconductor [5]. A variety of theoretical and experimental works have been devoted to establishing it, but it turns out after a decade of its discovery [6] that it is extremely difficult to identify the spin structure of a Cooper pair although the gap structure with line node is well established now. For example, it is pointed out that recent phase-sensitive experiments by Nelson *et al.* [7], Kidwingira *et al.* [8] and Xia *et al.* [9], all of which claim a triplet pairing, are also explained in terms of the singlet scenario by Zutic and Mazin [10] and Mineev [11]. The most direct and virtually only probe to detect its parity is the KS experiment. In fact KS experiments using various nucleus, such as ^{87}Sr , ^{101}Ru , ^{99}Ru and ^{17}O atoms, fail to pin down the spin direction of pairs, i.e. orientation of the d -vector because of the invariance of KS for both field directions of c - and ab -axes as low as $H = 200\text{G}$ [12]. There is no field direction where KS changes below T_c . Thus at present it is fair to say that the two scenarios either based on singlet and triplet pairings are still under debate. Note that the appearance of magnetic field below T_c associated with spontaneous time reversal symmetry breaking observed by μSR experiment [13] is explained

equally by spin singlet scenario as well as triplet one [14].

We examine the parity issue in Sr_2RuO_4 through analyses of the specific heat experiment by Deguchi *et al.* [16] under various T and H . There are several outstanding problems posed by this experiment, whose understanding leads to a new clue for this debate. One of the most interesting discoveries is why the field dependence of the Sommerfeld coefficient $\gamma(H) = \lim_{T \rightarrow 0} C/T$ (C is the specific heat) in the basal plane shows a concave curvature in spite of the existence of the line node gap. Namely, this is quite at odd because $\gamma(H)$ is expected to be a \sqrt{H} -like behavior with a convex curvature due to line nodes, i.e. the so-called Volovik effect [15]. It is remarkable to see that the concave curve becomes a Volovik \sqrt{H} curve with a convex curvature when the direction of the applied field moves away only by a few degrees of angle θ from the basal ab -plane (see inset (a) in Fig.3). In addition to analyses of the specific heat data [16] we also examine magnetization data [17] at low temperatures under a field. We explain these experiments based on an idea that strong Pauli paramagnetic effect is important in the basal ab plane physics of Sr_2RuO_4 and establish a consistent picture for its superconductivity.

We calculate the vortex lattice state properties by quasiclassical Eilenberger theory in the clean limit [18]. This framework is valid when $k_F \xi \gg 1$ (k_F Fermi wave number and ξ coherent length), which is satisfied by Sr_2RuO_4 . We include the paramagnetic effects due to the Zeeman term $\mu_B B(\mathbf{r})$. The flux density of the internal field is $B(\mathbf{r})$ and μ_B is a renormalized Bohr magneton [19]. The quasiclassical Green's functions $g(\omega_l + i\tilde{\mu}B, \mathbf{k}, \mathbf{r})$, $f(\omega_l + i\tilde{\mu}B, \mathbf{k}, \mathbf{r})$ and $f^\dagger(\omega_l + i\tilde{\mu}B, \mathbf{k}, \mathbf{r})$ are calculated in the vortex lattice state by the Eilenberger equation

$$\begin{aligned} \{\omega_n + i\tilde{\mu}B + \tilde{\mathbf{v}}(\mathbf{k}_F) \cdot [\nabla + i\mathbf{A}(\mathbf{r})]\} f &= \Delta(\mathbf{r})g, \\ \{\omega_n + i\tilde{\mu}B - \tilde{\mathbf{v}}(\mathbf{k}_F) \cdot [\nabla - i\mathbf{A}(\mathbf{r})]\} f^\dagger &= \Delta^*(\mathbf{r})g, \end{aligned}$$

where $g = (1 - ff^\dagger)^{1/2}$, $\text{Reg} > 0$, and the normalized Fermi velocity $\tilde{\mathbf{v}}$ is introduced so that $\langle \tilde{\mathbf{v}}^2 \rangle_{\mathbf{k}} = 1$ where $\langle \cdots \rangle_{\mathbf{k}}$ indicates the Fermi surface average. The paramagnetic parameter is $\tilde{\mu} = \mu_B B_0 / \pi k_B T_c$. We consider the d -wave pairing for a pairing function with line

nodes on the two-dimensional (2D) cylindrical Fermi surface. The pair potential is selfconsistently calculated. The vector potential \mathbf{A} for the internal magnetic field is selfconsistently determined by considering both the diamagnetic contribution of supercurrent and the contribution of the paramagnetic moment. We consider the large Ginzburg-Landau parameter $\tilde{\kappa} = 20$. The local density of states is given by $N(\mathbf{r}, E) = N_{+1}(\mathbf{r}, E) + N_{-1}(\mathbf{r}, E)$ with $N_{\sigma}(\mathbf{r}, E) = \langle \text{Re}\{g(\omega_l + i\sigma\tilde{\mu}B, \mathbf{k}, \mathbf{r})|_{i\omega_l \rightarrow E+i\eta}\} \rangle_{\mathbf{k}}$ for each spin component $\sigma = \pm 1$. We typically use $\eta = 0.01$. The density of states is obtained by its spatial average as $N(E) = \langle N(\mathbf{r}, E) \rangle_{\mathbf{r}}$, which is identified as the Sommerfeld coefficient $\gamma(H)$ in specific heat at lower T . Using the Doria-Gubernatis-Rainer scaling, we calculate magnetization M including diamagnetic and paramagnetic contributions. The details are found in Refs. [18, 19].

The paramagnetic parameter $\tilde{\mu} \propto H_{c2}^{\text{orb}}/H_p$, which is a key parameter to analyze $\gamma(H)$, is related to the ratio of the hypothetical orbitally limited upper critical field H_{c2}^{orb} and the Pauli limiting field $H_p = \Delta_0/\sqrt{2}\mu_B$ (Δ_0 is the gap amplitude at $T = 0$). H_p is a material-specific bulk parameter independent of the field orientation evidenced by nearly isotropic bulk susceptibility observed [5]. The angle-dependence of the paramagnetic parameter $\tilde{\mu}(\theta)$ comes through the factor: $H_{c2}^{\text{orb}}(\theta)$. This orbital-limited $H_{c2}^{\text{orb}}(\theta)$ is sensitive to the field orientation for highly anisotropic system such as in the present layered material; Sr_2RuO_4 .

The reduction of H_{c2} from H_{c2}^{orb} due to the paramagnetic effect is obtained by solving the Eilenberger equation as $H_{c2}(\tilde{\mu}) = H_{c2}^{\text{orb}}/\sqrt{1 + 2.4\tilde{\mu}^2}$. This is derived originally in dirty limit s -wave case [21], but we confirm it to be valid numerically in the present clean limit d -wave case too as seen from Fig. 1 where the calculated values are compared with this expression.

It is natural to consider that $H_{c2}^{\text{orb}}(\theta)$ is described by the effective mass model, namely $H_{c2}^{\text{orb}}(\theta)/H_{c2||ab}^{\text{orb}} = 1/\sqrt{\Gamma^2 \sin^2 \theta + \cos^2 \theta}$ which simply embodies the fact that the orbital motion of electrons is determined by the directional cosine of the field to the basal plane. The anisotropy $\Gamma = H_{c2||ab}^{\text{orb}}/H_{c2||c}^{\text{orb}}$ is an unknown parameter here. But it is assigned by the requirement that the experimental $H_{c2}(\theta)$ be reproduced theoretically. Namely, once Γ is determined, the angle dependence of $H_{c2}(\theta)$ is automatically known through the angle dependence of the paramagnetic parameter $\tilde{\mu}(\theta)$, which controls the reduction of the upper critical field H_{c2} from the ‘‘hypothetical’’ orbital-limited field H_{c2}^{orb} .

Having known the paramagnetic depairing effect on $H_{c2}(\tilde{\mu})$, we can calculate the angle dependence of the observed $H_{c2}(\theta)$ where we take account of the fact that $\tilde{\mu} \propto H_{c2}^{\text{orb}}/H_p$ is θ -dependent through the factor $H_{c2}^{\text{orb}}(\theta)$ given above. Thus we obtain $\tilde{\mu}(\theta) = \tilde{\mu}_0/\sqrt{\Gamma^2 \sin^2 \theta + \cos^2 \theta}$ with $\tilde{\mu}_0$ being the value at $\theta = 0$. By combining these relations, we finally obtain the θ dependence of the ob-

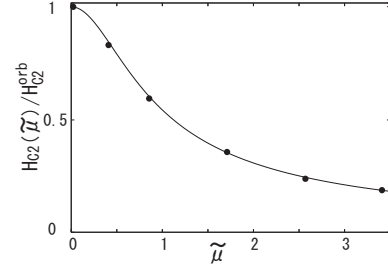


FIG. 1: Reduction of $H_{c2}(\tilde{\mu})$ as a function of $\tilde{\mu}$ evaluated by quasiclassical Eilenberger equation. The fitting curve is described well by $H_{c2}(\tilde{\mu})/H_{c2}^{\text{orb}} = 1/\sqrt{1 + 2.4\tilde{\mu}^2}$.

served $H_{c2}(\theta)$ as $H_{c2}(\theta) = 1/\sqrt{\Gamma^2 \sin^2 \theta + \cos^2 \theta + 2.4\tilde{\mu}_0}$. This takes account of both orbital- and paramagnetic depairing effects simultaneously. In order to reproduce the observed anisotropy $\Gamma^{\text{obs}} = 20$, we find $\tilde{\mu}_0 = 3.41$ when $\Gamma = 107$. Note that $\tilde{\mu}_0$ and Γ are not independent parameters. As shown in Fig. 2 our effective mass model with the paramagnetic effect explains the angle dependence of $H_{c2}(\theta)$ once we fix one adjustable parameter. It is to be noted as shown in inset of Fig. 2 the $\tilde{\mu}(\theta)$ value is completely determined by the effective mass form with $\Gamma = 107$.

As for the assigned $\Gamma = 107$ we point out that the diamagnetic orbital current is determined by the perpendicular component of the average Fermi velocity to the field direction. Thus Γ is the anisotropy ratio of the Fermi velocities, namely $\Gamma = \sqrt{\langle v_{F||c}^2 \rangle / \langle v_{F||ab}^2 \rangle}$. This quantity is determined directly by dHvA experiment; $\Gamma_{\alpha} = 117$, $\Gamma_{\beta} = 57$ and $\Gamma_{\gamma} = 174$ for three bands α , β and γ respectively [5]. Note that a simple geometric average $\Gamma_{\text{eff}} = \frac{1}{3}(\Gamma_{\alpha} + \Gamma_{\beta} + \Gamma_{\gamma}) = 116$ is well compared with our assignment $\Gamma = 107$. In this sense there is virtually no adjustable parameter in our analysis. In passing we note that the observed ratio $\Gamma^{\text{obs}} = H_{c2||ab}/H_{c2||c} = 20$ is strongly reduced from Γ_{eff} , apparently suggesting some reduction mechanism. We clarified it here.

Let us now come to our main discussions on the analyses of the specific heat at a low T . In Fig. 3 we display $\gamma(H)$ for several values of $\tilde{\mu}$ together with the experimental data in inset (a) for various θ values. They show strikingly similar behaviors as a whole. The larger angle data exhibit a strong upward curvature, corresponding to the conventional $\gamma(H) \sim \sqrt{H}$ which is characteristic to the line node gap structure. Those are reproduced in our $\tilde{\mu}=0.02$, or 0.41 curves. As θ becomes smaller, this changes into almost linear or concaved curves near H_{c2} . This behavior is captured by the theoretical calculations for larger $\tilde{\mu}$'s. Thus the overall ‘‘metamorphosis’’ of $\gamma(H)$ from the conventional \sqrt{H} to a strong convex curve is reproduced by increasing $\tilde{\mu}$. As shown in inset (b) of Fig. 3, the data are fitted well by our calculations near H_{c2} where we have used the $\tilde{\mu}(\theta)$ values determined

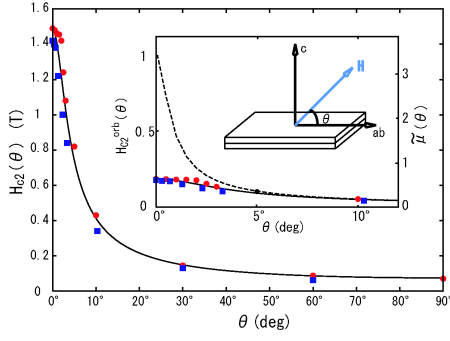


FIG. 2: (color online) Calculated angle dependence of $H_{c2}(\theta)$ (solid line). Circles [16] (squares [20]) are experimental data. Enlarged figure is shown in inset for small angles. The dotted line is the original orbital limit $H_{c2}^{orb}(\theta)$ of the effective mass form with $\Gamma = 107$. The dotted line also shows $\tilde{\mu}(\theta)$ with $\tilde{\mu}_0 = 3.41$ (right hand scale). θ is the angle from the ab plane.

above (see the inset of Fig. 2 with $\tilde{\mu}_0 = 3.41$). We have computed the six cases shown in Fig.3 for $\tilde{\mu}$ values and obtained $\gamma(H)$ for other $\tilde{\mu}$'s by interpolation.

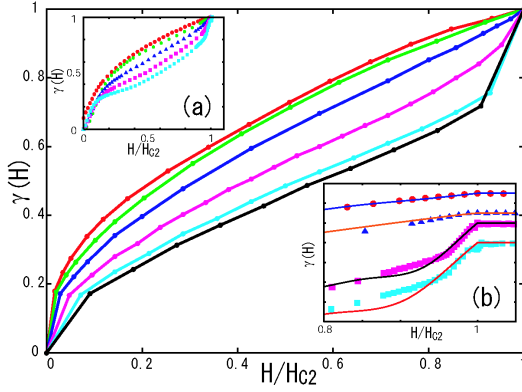


FIG. 3: (color online) Zero-energy DOS $\gamma(H)$ at $T = 0.1T_c$ for $\tilde{\mu} = 0.02, 0.41, 0.86, 1.71, 2.57$ and 3.41 from top to bottom. Inset (a) shows the experimental data [16] for $\theta = 0^\circ, 2.5^\circ, 3.0^\circ, 5.0^\circ$ and 90° from bottom to top. Inset (b) is the fitting of the data $\theta = 0^\circ$ by $\tilde{\mu} = 3.41$, 0.5° ($\tilde{\mu} = 2.36$), 5° ($\tilde{\mu} = 0.33$) and 90° ($\tilde{\mu} = 0.03$) from bottom to top, which are shifted upwards.

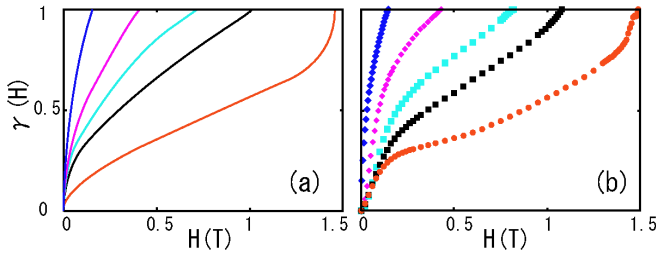


FIG. 4: (color online) (a) $\gamma(H)$ for $\tilde{\mu} = 3.41, 0.60, 0.36, 0.18$ and 0.06 from bottom to top. (b) Corresponding data [16] for $\theta = 0^\circ, 3^\circ, 5^\circ, 10^\circ$ and 30° .

In Fig. 4 we display the theoretical $\gamma(H)$ behaviors (a) and the corresponding specific heat data [16] (b), where we read off $\tilde{\mu}(\theta)$ from the inset of Fig.2. Our theoretical curves explain these data in a consistent manner. In particular, it is noteworthy; (1) At $\theta = 0^\circ$ where $\tilde{\mu}(0) = \tilde{\mu}_0 = 3.41$ is largest, $\gamma(H)$ shows a \sqrt{H} -like sharp rise in smaller H region because of the presence of line nodes. But it is limited only to lower fields. (2) In the intermediate wide field region ($0.5T < H < 1T$), $\gamma(H)$ exhibits an almost linear change in H . This extended linear change is shown to be consistent thermodynamically with magnetization $M(T, H)$ behavior as seen shortly. (3) In the high field region ($H > 1T$) towards $H_{c2} = 1.5T$, $\gamma(H)$ displays a sharp rise with a strong concave curvature. As H increases, the Pauli effect proportional linearly to H becomes growingly effective, modifying $\gamma(H)$ from usual \sqrt{H} to a concave H^α -like curve with $\alpha > 1$.

The data for $\theta = 3^\circ$ where $\tilde{\mu}(\theta = 3^\circ) = 0.60$ show a similar behavior to that at $\theta = 0^\circ$, but the features associated with the Pauli effect, namely, the existence of the inflection point from convex to concave curves and sharp rise towards H_{c2} are weakened. The $\gamma(H)$ data for higher angles ($\theta > 3^\circ$) exhibit an intermediate behavior between those at $\theta = 0^\circ$ and the ordinary \sqrt{H} curve, continuously changing its shape with θ . It is remarkable that the strong concave curves of the experimental data for small angles, which were unexplained before, are reproduced by the Pauli paramagnetic effect. Physically, this effect makes the conventional Abrikosov vortex state unstable, ultimately leading to the normal state via a first order transition or the FFLO state. The sharp rise in $\gamma(H)$ near H_{c2} is a precursor to it.

In Fig. 5 we show the calculated results of magnetization $M(H)$ for several T 's (a) together with the experimental data [17] (b) to qualitatively understand the paramagnetic effects on $M(T, H)$. We do not attempt to reproduce the data quantitatively because the data are in a qualitative nature due to hysteresis effects. It is seen from Fig. 5(a) that the magnetization with a convex curvature at lower field changes into that with a concave one towards H_{c2} . There is an inflection point field H_K in between. The relative position of H_K to each H_{c2} decreases with T (also see insets). In higher T 's H_K becomes invisible because of thermal effect. These two features are observed experimentally as seen from Fig. 5(b). The inflection point field H_K roughly coincides with that in $\gamma(H)$ as seen from Fig. 4, implying that these are thermodynamically related to each other.

As is seen from Fig.5 upon lowering T the slope of $M(H)$ at H_{c2} becomes steeper, meaning that κ_2 decreases, instead of increases as in usual superconductors [21]. This is another obvious supporting evidence that the paramagnetic effect is important in Sr_2RuO_4 .

It is easy to derive a thermodynamic Maxwell relation $\frac{d}{dH} \frac{C}{T} = \frac{\partial^2}{\partial T^2} M(T, H)$ from which we can see at low

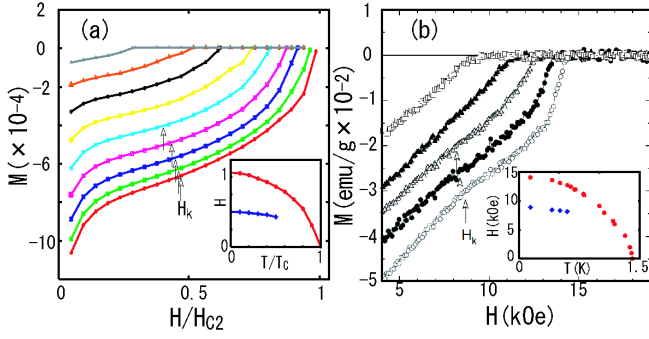


FIG. 5: (color online) (a) Calculated magnetization curves for various $T/T_c = 0.1, 0.2, 0.3 \dots, 0.9$ from bottom to top for $\tilde{\mu} = 1.71$. Inset shows H_{c2} and the inflection point H_K . (b) Corresponding data [17] for $T/T_c = 0.1, 0.28, 0.40$ and 0.56 from bottom to top for $H \parallel ab$. Inset shows H_{c2} and “kink” field H_K in their terminology [17]. Magnetization of the normal paramagnetic moment is subtracted.

T , $\frac{\partial \gamma(H)}{\partial H} = \beta(H)$ with $M(T, H) = M_0(H) + \frac{1}{2}\beta(H)T^2$. We estimate $\beta(H)$ from the experimental data [17] in Fig. 5, finding that $\beta(H) \sim \text{const}$ for $0.5T < H < 1T$ and $\beta(H) \propto H^3$ for $1T < H < 1.35T$. This implies that $\gamma(H) \propto H(H^4)$ for $0.5T < H < 1T$ ($1T < H < 1.35T$). These behaviors in $\gamma(H)$ are indeed seen for the $\theta = 0^\circ$ data shown in Fig. 4. These analyses, which are free from any microscopic model, mean that the mysterious behavior of $\gamma(H)$ is supported to be true thermodynamically and comes from the intrinsic nature deeply rooted to the superconductivity in Sr_2RuO_4 .

There are several known difficulties associated with the most popular two component chiral p -wave pairing; $\hat{z}(p_x + ip_y)$ [22] or $\hat{z}(p_x + ip_y) \cos p_z$ [23]: Experimentally these triplet states are unable to explain the paramagnetic effects mentioned above because the d -vector is not locked in the basal plane. Theoretically these states give a large in-plane H_{c2} anisotropy[24] which is not observed. The present singlet scenario is free from it.

Let us go on considering the high field phase for $H \parallel ab$ observed as the double transition[20]. It appears in a narrow H - T region along $H_{c2 \parallel ab}$, starting at $T_0 = 0.8K$, or $T_0 = 0.53T_c$ at which three transition lines meet, giving rise to a tricritical point in H vs. T plane. T_0 is remarkably similar to the so-called Lifshitz point $T_L = 0.56T_c$ in the FFLO phase diagram for a Pauli limited superconductor where the orbital depairing is quenched completely. This number $T_L = 0.56T_c$ is universal, valid for a variety of situations, including 3D Fermi sphere s -wave[25], 2D s -wave[26] and d -wave[27], and 1D s -wave[28] models. Our identified large paramagnetic parameter $\tilde{\mu} = 3.41$ means that our system is in almost Pauli limiting where the orbital effect is almost perfectly quenched because the two-dimensionality in Sr_2RuO_4 is so extreme. In fact note that the identified anisotropy $\Gamma = 107$ implies $H_{c2 \parallel ab}^{\text{orb}} \sim 7.5T$ which is

reduced to $H_{c2 \parallel ab} = 1.5T$ by the Pauli effect. Thus we propose here to identify this high field phase as FFLO.

The extreme two-dimensionality is obvious: If H is tilted away from the ab plane only by $\theta > 0.3^\circ$, the double transition vanishes[20]. According to Nakai, *et al.*[29] the FFLO region at low T occupies $\sim 0.8\%$ below H_{c2} , which is comparable with the width $\sim 200G$ of the high field phase below $H_{c2 \parallel ab} = 1.5T$, a region $200G/1.5T \sim 1.3\%$ [20]. Guided by the known phase diagram[21], we predict that as the field orientation θ increases, $\tilde{\mu}$ decreasing, this high field phase survives only for $0 < \theta < 0.3^\circ$ and quickly diminishes for $\theta > 0.3^\circ$. At around $\theta \sim 1.0^\circ$ there appears a first order transition along H_{c2} line instead of FFLO. Then for $\theta > 2.0^\circ$ it also disappears above which the paramagnetic effect becomes ineffective and Sr_2RuO_4 is described by a conventional singlet superconductor with line nodes. These predictions based on our analyses are all testable experimentally although the details should be further sharpened theoretically.

In conclusion, we have analyzed both specific heat at lower T and magnetization $M(T, H)$ by self-consistently solving microscopic quasi-classical Eilenberger equation for the gap function with line nodes. It is seen that the Pauli paramagnetic depairing effect is essential in understanding the data in Sr_2RuO_2 . This is possible only for either singlet pairing, or triplet pairing with the d vector locked in the basal plane.

We are grateful for useful discussions and communications to K. Deguchi, K. Tenya, K. Ishida, Y. Maeno, H. Adachi, N. Nakai, P. Miranovic and Y. Matsuda. M. Tsutsumi helps us for preparing figures.

-
- [1] K. Machida, Prog. Theor. Phys. Suppl. **108**, 229 (1992). J.A. Sauls, Adv. Phys. **43**, 113 (1994). R. Joynt and L. Taillefer, Rev. Mod. Phys. **74**, 235 (2002).
 - [2] See for recent progress: K. Machida *et al.*, J. Phys. Soc. Jpn. **68**, 3364 (1999).
 - [3] A.J. Leggett, Rev. Mod. Phys. **47**, 331 (1975).
 - [4] H. Tou, *et al.*, Phys. Rev. Lett. **80**, 3129 (1998).
 - [5] A.P. Mackenzie and Y. Maeno, Rev. Mod. Phys. **75**, 657 (2003).
 - [6] Y. Maeno, *et al.*, Nature (London) **372**, 532 (1994).
 - [7] K.D. Nelson, *et al.*, Science **306**, 1151 (2004).
 - [8] F. Kidwingira, *et al.*, Science **314**, 1267 (2006).
 - [9] J. Xia, *et al.*, Phys. Rev. Lett. **97**, 167002 (2006).
 - [10] I. Zutic and I. Mazin, Phys. Rev. Lett. **95**, 217004 (2005).
 - [11] V.P. Mineev, arXiv: cond-mat/0703624.
 - [12] See for recent paper and cited therein: H. Murakawa, *et al.*, Phys. Rev. Lett. **93**, 167004 (2004).
 - [13] G.M. Luke, *et al.*, Nature (London) **394**, 558 (1998).
 - [14] See the recent result on this topic: J.R. Kirtley, *et al.*, arXiv: 0704.3364, showing null result of spontaneous moment problem.
 - [15] G.E. Volovik, JETP Lett., **58**, 469 (1993).
 - [16] K. Deguchi, *et al.*, J. Phys. Soc. Jpn. **73**, 1313 (2004).

- [17] K. Tenya, *et al.*, J. Phys. Soc. Jpn. **75**, 023702 (2006).
- [18] M. Ichioka, *et al.*, Phys. Rev. B **59**, 8902 (1999).
- [19] H. Adachi, *et al.*, J. Phys. Soc. Jpn. **74**, 2181 (2005).
- [20] K. Deguchi, *et al.*, J. Phys. Soc. Jpn. **71**, 2839 (2002).
- [21] D. Saint-James, *et al.*, in *Type II Superconductivity* (Pergamon, 1969, Oxford) p. 171.
- [22] T.M. Rice and M. Sigrist, J. Phys.: Condens. Matter **7**, L643 (1995).
- [23] Y. Hasegawa, *et al.*, J. Phys. Soc. Jpn. **69**, 336 (2000).
- [24] K. Machida, *et al.*, J. Phys. Soc. Jpn. **54**, 1552 (1985).
- R.P. Kauer, *et al.*, Phys. Rev. B **72**, 144528 (2005).
- [25] S. Takada and T. Izuyama, Prog. Theor. Phys. **41**, 635 (1969).
- [26] H. Shimahara, Phys. Rev. B **17**, 12760 (1994).
- [27] A.B. Vorontsov, *et al.*, Phys. Rev. B **72**, 184501 (2005).
- [28] K. Machida and H. Nakanishi, Phys. Rev. B **30**, 122 (1984).
- [29] N. Nakai, *et al.*, private communication.